



# CHORUS

This is the accepted manuscript made available via CHORUS. The article has been published as:

## Plasmonic Landau damping in active environments

Niket Thakkar, Nicholas P. Montoni, Charles Cherqui, and David J. Masiello

Phys. Rev. B **97**, 121403 — Published 12 March 2018

DOI: [10.1103/PhysRevB.97.121403](https://doi.org/10.1103/PhysRevB.97.121403)

# Plasmonic Landau Damping in Active Environments

Niket Thakkar,<sup>1,\*</sup> Nicholas P. Montoni,<sup>2</sup> Charles Cherqui,<sup>2</sup> and David J. Masiello<sup>1,2,†</sup>

<sup>1</sup>*Department of Applied Mathematics, University of Washington, Seattle, Washington 98195-3925, USA*

<sup>2</sup>*Department of Chemistry, University of Washington, Seattle, Washington 98195-1700, USA*

(Dated: February 26, 2018)

Optical manipulation of charge on the nanoscale is of fundamental importance to an array of proposed technologies, from selective photocatalysis to nanophotonics. Open plasmonic systems, where collective electron oscillations release energy and charge to their environments, offer a potential means to this end as plasmons can rapidly decay into energetic electron-hole pairs; however, isolating this decay from other plasmon-environment interactions remains a challenge. Here we present an analytic theory of noble metal nanoparticles that quantitatively models plasmon decay into electron-hole pairs, demonstrates that this decay depends significantly on the nanoparticle's dielectric environment, and disentangles this effect from competing decay pathways. Using our approach to incorporate embedding material and substrate effects on plasmon-electron interaction, we show that predictions from the model agree with four separate experiments. Finally, examination of coupled nanoparticle-emitter systems further shows that the hybridized in-phase mode more efficiently decays to photons while the out-of-phase mode more efficiently decays to electron-hole pairs, offering a new strategy to tailor open plasmonic systems for charge manipulation.

19 Localized surface plasmon (LSP) resonances, the collective oscillations of conduction-band electrons in noble metal  
 20 nanoparticles (MNPs), have a fundamental role in nanoscale optics and electronics<sup>1</sup>. These collective phenomena offer  
 21 unique control of light<sup>1,2</sup>, heat<sup>3,4</sup>, and charge<sup>5,6</sup> in nanoscale systems, and studies of their basic properties continue  
 22 to promise new applications in a range of fields, from selective catalysis<sup>7</sup> to quantum computing<sup>8</sup>. The intercon-  
 23 version of LSPs to individual electronic excitations, so-called Landau damping<sup>9</sup>, has gained particular experimental  
 24 interest<sup>5,10–13</sup>. Studies report changes in LSP spectra due to changes in particle environment, such as substrate or  
 25 embedding material<sup>11–13</sup>, as potential signatures of enhanced interconversion rates, indicating that Landau damping  
 26 depends on the MNP’s dielectric environment in analogy to Purcell enhancement of a fluorescent molecule’s radiative  
 27 decay<sup>14</sup>. Still, disentangling Landau damping from other effects such as optical energy transfer<sup>15</sup> presents significant  
 28 experimental challenges and complicates the interpretation of results. A theory of LSP-electron interaction capable  
 29 of incorporating environmental effects, from substrates to other optical emitters, is needed to guide experiments and  
 30 offer a platform to optimize nanoparticle systems for electron-hole pair generation.

31 Landau damping is known to increase with decreasing MNP size<sup>16–18</sup> and is most significant at length scales  
 32 where classical descriptions of LSPs require quantum-mechanical modification. Recent research on MNPs<sup>19–22</sup>, MNP  
 33 aggregates<sup>23</sup>, and bulk metals<sup>24–27</sup> has confirmed this result while emphasizing the importance of an accurate de-  
 34 scription of the metal’s electronic structure, electron spill-out, and nonlocal dielectric effects. Meanwhile, a large  
 35 body of research has taken quantum descriptions of small metal clusters and has worked to develop atomistic models  
 36 of LSPs in larger clusters<sup>28–35</sup>. In most cases, however, MNPs are described in isolation, and the incorporation of  
 37 environmental effects is often computationally intractable.

38 In this paper, we present a quantitatively accurate, analytic theory of Landau damping in noble metals, accounting  
 39 for optically active environments. We compare the theory to four experiments: the photofragmentation spectroscopy  
 40 by Tiggesbäumker et al.<sup>36</sup> on silver clusters in vacuum, the matrix deposition spectroscopies by Charlé et al.<sup>37</sup> and  
 41 Harbich et al.<sup>38</sup> on silver clusters in argon, and the electron energy-loss spectroscopy (EELS) by Scholl et al.<sup>39</sup> on  
 42 silver nanospheres on 3 nm carbon substrates. After incorporating dielectric background and substrate effects, we  
 43 demonstrate that the theory reproduces the observed LSP energies in all four experiments over decades of cluster sizes,  
 44 from  $\sim 245,000$  atoms to 5 atoms, reconciling experiments previously thought to disagree<sup>28</sup> and showing environmental  
 45 effects’ role in determining quantum LSP properties. We conclude by generalizing the theory to predict the quantum-  
 46 corrected energies of hybrid LSP-emitter systems relevant to studies of nanoparticle assemblies<sup>40</sup>, MNP-quantum dot  
 47 systems<sup>41</sup>, and LSP-enhanced molecular spectroscopies<sup>42</sup>. Surprisingly, we find that unlike the radiative properties of  
 48 LSP-emitter systems<sup>43</sup>, the hybridized out-of-phase LSP-emitter mode decays to electron-hole pairs most efficiently,  
 49 and we suggest future experiments to measure this effect.

50 To elucidate the mechanism by which LSPs disintegrate into electron-hole pairs, we first consider an isolated silver  
 51 nanosphere. The inset of Fig. 1a depicts a sphere with radius  $a$  characterized by infinite frequency dielectric response  
 52  $\varepsilon_1$ , modeling screening due to core electrons<sup>16,18,39</sup>, and plasma frequency  $\omega_p$  embedded in material with dielectric  
 53 constant  $\varepsilon_2$ . Both  $\varepsilon_1$  and  $\omega_p$  are estimated by fitting a frictionless, free-electron (Drude) model to optical frequency  
 54 dielectric data<sup>45</sup> for bulk silver<sup>46</sup>.

55 In the SI<sup>46</sup>, we consider conduction electrons confined to the MNP by a potential  $U_+(\mathbf{x})$  and show that their mean-  
 56 field Coulomb interaction gives rise to a set of multipolar oscillators corresponding to particle-localized collective

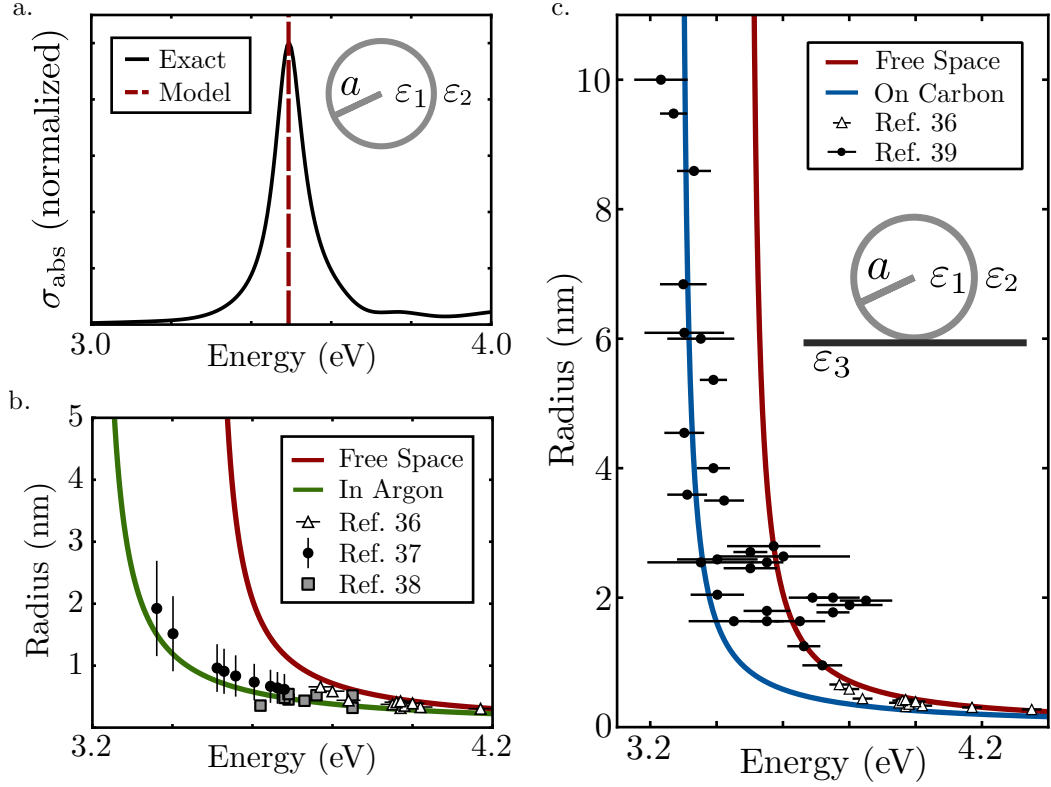


FIG. 1. Predictions and validations of the model. (a) The silver nanosphere’s (inset) absorption cross section is computed with Mie theory (black curve) and compared to  $\hbar\omega_{10}$  (red dashed line) for  $a = 10$  nm and  $\epsilon_2 = 1$ , confirming the model’s reproduction of classical results. (b) Comparison of the free space ( $\epsilon_2 = 1$ , red line) and argon embedded ( $\epsilon_2 = 1.7^{44}$ , green line) LSP energy to photofragmentation spectroscopy in vacuum (white triangles, 1 standard deviation error bars)<sup>36</sup> and matrix deposition spectroscopies<sup>37,38</sup> in argon (black circles with 1 standard deviation error bars and grey boxes). Quantitative agreement between the theory and experiments shows that the theory effectively incorporates embedding dielectric effects. (c) Comparison of the LSP energy to EELS on a carbon substrate (black circles, 2 standard deviation error bars)<sup>39</sup> with data from<sup>36</sup> for reference. When the model is extended to incorporate the carbon substrate (blue curve,  $\epsilon_2 = 1, \epsilon_3 = 3$ ), the predicted renormalized LSP energies agree excellently with measurement.

57 election motion, so-called LSPs<sup>47</sup>. The system’s Hamilton is

$$H_{\text{free}} = \sum_i \left[ \frac{\mathbf{p}_i^2}{2m_e} + U_+(\mathbf{x}_i) \right] + \sum_{\ell m} \left( \frac{V_{\ell m}}{2} |p_{\ell m}|^2 + \frac{\omega_{\ell m}^2}{2V_{\ell m}} |q_{\ell m}|^2 \right) - \frac{e}{2m_e c} \sum_i [\mathbf{p}_i \cdot \mathbf{A}(\mathbf{x}_i) + \mathbf{A}(\mathbf{x}_i) \cdot \mathbf{p}_i], \quad (1)$$

58 where  $q_{\ell m}$  and  $p_{\ell m}$  are generalized LSP coordinates and momenta defined by the total conduction electron density’s  
 59 projection onto the  $\ell, m$  multipole moments’ field within the nanosphere. When retardation effects across the MNP  
 60 are neglected<sup>18</sup>, these projections oscillate with frequencies  $\omega_{\ell m} = \sqrt{\ell\omega_p^2 / (\ell\epsilon_1 + (\ell+1)\epsilon_2)}$ , and mode volumes  $V_{\ell m} =$   
 61  $[3/(\ell\epsilon_1 + (\ell+1)\epsilon_2)]V_s$  where  $V_s$  is the sphere’s volume. Eq. 1 also introduces the electron positions,  $\mathbf{x}_i$ , and momenta,  
 62  $\mathbf{p}_i$ , which couple to the collective motion through  $\mathbf{A}(\mathbf{x})$ , the LSP vector potential. It is this interaction that governs  
 63 Landau damping.

64 The validity of our estimates of  $\epsilon_1$  and  $\omega_p$  can be assessed by comparing the model’s prediction for the LSP energy<sup>46</sup>  
 65 with that from Mie theory<sup>48</sup>, the exact solution to Maxwell’s equations for a dielectric sphere. This is done in Fig.  
 66 1a, where the model’s predicted absorption resonance under  $z$ -polarized, plane-wave excitation (red dashed line) is  
 67 compared to the Mie solution for an  $a = 10$  nm silver nanosphere computed with complex-valued bulk dielectric data<sup>45</sup>

(black line). We see that the predicted resonance energy agrees with the exact solution, and that the excitation source selects only the  $\ell = 1, m = 0$  LSP mode, confirming that the MNP's optical properties are dipole-dominated at small radii<sup>16,18,39</sup>.

We now quantize  $H_{\text{free}}$  and calculate the leading order effects of electron-plasmon interaction perturbatively.  $U_+(\mathbf{x})$  is modeled as an infinite spherical well, and the resulting electron wave functions and energies are specified in Ref.<sup>16</sup>. While this approximation neglects complexity of silver's band structure and electron spill-out at small sizes, an important effect in alkali metals<sup>22</sup>, we show below that this greatly simplified electronic structure is sufficient for describing environmental effects on the noble MNPs of interest here.

To calculate the decay rate for LSPs to electron-hole pairs, we consider transitions between the initial and final Fock states  $|\varphi_i\rangle = |1_{10}; 0_e, 0_h\rangle$  and  $|\varphi_f\rangle = |0_{10}; 1_e, 1_h\rangle$  of the form  $|N_{\ell m}; n_e, n_h\rangle$  with  $N_{\ell m}$  plasmons in the  $\ell, m$  mode, and  $n_e$  ( $n_h$ ) electrons (holes) with quantum numbers  $e$  ( $h$ ). All omitted occupation numbers are equal to zero, and the restriction to  $\ell = 1, m = 0$  is made based on the discussion of Fig. 1a.

Using Fermi's golden rule with the interaction Hamiltonian in Eq. 1, we find the LSP decay rate to electron-hole pairs<sup>46</sup>

$$\Gamma_{\text{free}}(\omega_{10}, V_{10}) = \frac{64V_{10}}{3\pi^3V_s} \frac{e^2}{\hbar a} \int_{x_0}^1 \frac{dx}{\nu^3} \sqrt{x^3(x+\nu)}, \quad (2)$$

where  $\nu = \hbar\omega_{10}/\epsilon_F$ ,  $\epsilon_F = 5.5$  eV is the Fermi-energy of silver<sup>16</sup>, and  $x_0 = \max\{0, 1 - \nu\}$ . Notice  $\Gamma_{\text{free}} \propto 1/a$ , demonstrating that Landau damping becomes more significant as MNP size decreases, in qualitative agreement with previous studies<sup>16-20</sup>.  $\Gamma_{\text{free}}$  can also be used to approximate the second-order change in LSP energy, resulting in the renormalized energy  $\hbar\omega_{10}^* \approx \sqrt{(\hbar\omega_{10} + \hbar\Gamma_{\text{free}})^2 - (\hbar\Gamma_{\text{free}}/2)^2}$ .

In Fig. 1b, we compare  $\hbar\omega_{10}^*$  to photofragmentation spectroscopy<sup>36</sup> of silver clusters in free space ( $\epsilon_2 = 1$ , red line) and to matrix deposition spectroscopies<sup>37,38</sup> of silver clusters embedded in argon ( $\epsilon_2 = 1.7^{44}$ , green line). We see that  $\hbar\omega_{10}^*$  rapidly blueshifts as  $a$  decreases in excellent agreement with the datasets, validating our approximations and indicating that our theory effectively incorporates the embedding dielectric. While not obvious, we show in the SI<sup>46</sup> that  $\Gamma_{\text{free}}$  increases with the embedding dielectric constant,  $\epsilon_2$ . Thus, LSP decay to electron-hole pairs is faster for MNPs in high dielectric materials since the plasmon field is more confined to the particle's interior and electron-plasmon interaction is therefore larger.

In Fig. 1c, we further compare  $\hbar\omega_{10}^*$  in free space (red line) to data obtained via EELS on a 3 nm carbon substrate<sup>39</sup>. The prediction only qualitatively agrees with the blueshift in the EELS data, generally overestimating the measured LSP energy. Although it is possible to modify  $\epsilon_1$  and  $\omega_p$  to shift our estimate to lower energy, this would be at the expense of agreement with Mie theory (Fig. 1a). This check is critical since simultaneous agreement with Mie theory and measurement at small sizes shows that the model correctly transitions from quantum to classical electrodynamics. Thus, we instead extend the theory to include substrate effects, demonstrating that the resulting LSP energies agree with Mie theory and all four experiments<sup>36-39</sup> simultaneously.

The  $\ell = 1, m = 0$  LSP field outside the MNP is identical to that of a point dipole located at the sphere's center<sup>46</sup>. This observation motivates using the method of images to incorporate the substrate. A point dipole with dipole moment  $\mathbf{d}$  located above an infinite plane with dielectric constant  $\epsilon_3$  induces an image dipole  $\mathbf{d}_I = -\mathbf{d}(\epsilon_3 - \epsilon_2)/(\epsilon_3 + \epsilon_2)$ , in the opposite direction for the experimentally relevant case  $\epsilon_3 > \epsilon_2^{15}$ . Although the substrates in experiments have

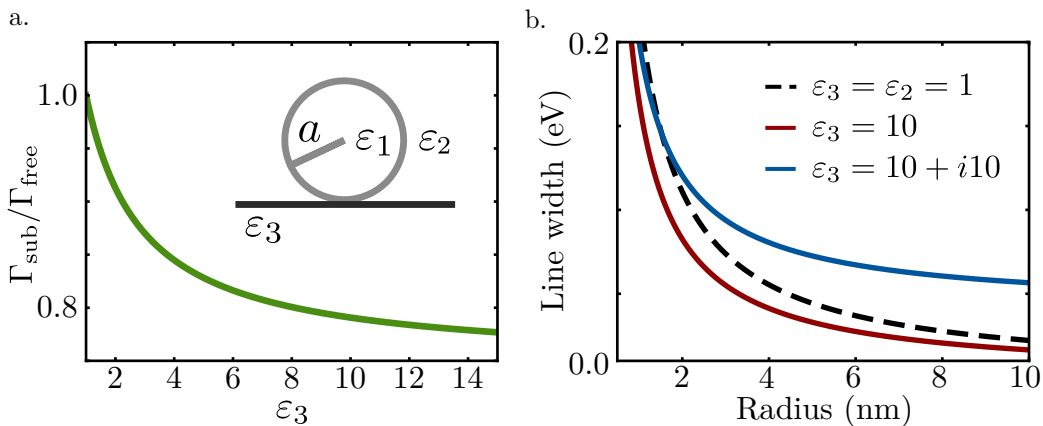


FIG. 2. (a) Substrate-dressed Landau damping relative to  $\Gamma_{\text{free}}$  as a function of  $\epsilon_3$ . Suppression of the decay rate quickly saturates as  $\epsilon_3$  increases. Thus, the change in optical properties from free space ( $\epsilon_3 = 1$ ) to any substrate ( $\epsilon_3 > 1$ ) is large compared to the change between low and high dielectric substrates. (b) Size dependence of the substrate-modified LSP linewidth accounting for LSP-electron interaction and intrinsic substrate losses. The black dashed line shows  $\Gamma_{\text{free}}$ , and if  $\epsilon_3$  is complex valued (blue curve), intrinsic substrate losses can cause an increase in linewidth, pushing the system into a regime where LSP decay to electron-hole pairs and to near-field interaction compete.

104 finite thickness, the dominant image contribution is that of the infinite half-space, which we verify by accounting for  
 105 the finite substrate in the SI<sup>46</sup>. Here, for simplicity, we model the substrate as infinite (Fig. 2a, inset), and we modify  
 106  $H_{\text{free}}$  to include  $\mathbf{d}_I$ ,

$$H_{\text{sub}} = H_{\text{free}} - \mathbf{d}_{10} \cdot \mathbf{E}_I - \frac{e}{2m_e c} \sum_i [\mathbf{p}_i \cdot \mathbf{A}_I(\mathbf{x}_i) + \mathbf{A}_I(\mathbf{x}_i) \cdot \mathbf{p}_i], \quad (3)$$

107 where  $\mathbf{d}_{10}$  is the LSP dipole moment and  $\mathbf{E}_I$  and  $\mathbf{A}_I$  are the image electric field and vector potential. Here it is evident  
 108 that the substrate affects the MNP both through LSP coupling and through modification of the vector potential within  
 109 the particle.

110 The LSP coupling can be diagonalized via transformation leading to a substrate-dressed LSP with mode volume  
 111  $\tilde{V}_{10} = V_{10} - 2g$  and resonance frequency  $\tilde{\omega}_{10} = \sqrt{\omega_{10}^2(1 - 2g/V_{10})}$  where  $g = \pi a^3(\epsilon_3 - \epsilon_2)(\epsilon_1 - \epsilon_2)^2/6(\epsilon_3 + \epsilon_2)(\epsilon_1 + 2\epsilon_2)^2$ ,  
 112 and we assume  $\mathbf{d}_{10}$  is parallel to the substrate. This indicates, in agreement with other studies<sup>13</sup>, that the LSP mode  
 113 volume and energy both decrease due to electrostatic substrate effects.

114 The remaining interaction term modifies the perturbation theory above. The LSP decay rate can be recalculated  
 115 under the approximation that the image vector potential operator,  $\mathbf{A}_I(\mathbf{x}_i)$ , can be treated as  $\mathbf{A}_I(\langle \mathbf{x}_i \rangle)$ . This ap-  
 116 proximation is valid since fluctuations of the electron position will destructively interfere as the number of electrons  
 117 increases. The perturbation theory gives

$$\begin{aligned} \Gamma_{\text{sub}}(\tilde{\omega}_{10}, \tilde{V}_{10}) &= |1 - \alpha|^2 \frac{64\tilde{V}_{10}}{3\pi^3 V_s} \frac{e^2}{\hbar a} \int_{\tilde{x}_0}^1 \frac{dx}{\tilde{\nu}^3} \sqrt{x^3(x + \tilde{\nu})} \\ &= |1 - \alpha|^2 \Gamma_{\text{free}}(\tilde{\omega}_{10}, \tilde{V}_{10}), \end{aligned} \quad (4)$$

118 for the substrate-modified rate of LSP decay into electron-hole pairs. Here  $\tilde{\nu} = \hbar\tilde{\omega}_{10}/\epsilon_F$ ,  $\tilde{x}_0 = \max\{0, 1 - \tilde{\nu}\}$ , and  
 119  $\alpha = (\epsilon_1 - \epsilon_2)(\epsilon_3 - \epsilon_2)/24(\epsilon_3 + \epsilon_2)$ .

120  $\Gamma_{\text{sub}}$  is compared to  $\Gamma_{\text{free}}$  for varying  $\epsilon_3$  in Fig. 2. Interestingly, in contrast to the  $\epsilon_2$  dependence of  $\Gamma_{\text{free}}$ , real-valued

121  $\varepsilon_3 > 1$  universally suppresses decay (Fig. 2a) since  $\mathbf{A}_I$  is opposite  $\mathbf{A}$  within the particle, screening the coupling to  
 122 electrons. Only when  $\varepsilon_3$  is complex-valued (Fig. 2b), indicating that the substrate has intrinsic losses, can energy  
 123 transfer result in an increase above the free space LSP linewidth, pushing the LSP into a regime where Landau  
 124 damping and near-field energy transfer become competitive. We stress, however, that this is due to intrinsic loss in  
 125 the substrate, not due to the enhancement of electron-hole pair generation, illustrating the difficulty in disentangling  
 126 these processes.

127 Using Eq. 4 we can calculate the quantum-corrected, substrate-dressed LSP energy as was done previously. This  
 128 is plotted in Fig. 1c (blue curve) with  $\varepsilon_3 = 3$  for carbon, and we see that the modified resonance energies agree  
 129 excellently with the EELS data<sup>39</sup> where the free space calculation fails. Since the previous calculation is simply a  
 130 special case ( $\varepsilon_3 = \varepsilon_2 = 1$ ) of Eq. 4, we have presented a single theory that quantitatively agrees with classical  
 131 electrodynamics and all four experiments<sup>36–39</sup> over a wide range of particle sizes.

132 Our theory explicitly models LSP-electron interaction and dielectric environment effects but neglects intrinsic losses  
 133 in bulk silver<sup>45</sup>, ligand effects, and electron spill-out, while using a local dielectric function and a relatively simple  
 134 approximation to the MNP electronic structure. This indicates that LSP-electron interaction dominates LSP loss  
 135 at these sizes and that environmental effects play a much more significant role in determining quantum plasmon  
 136 properties than previously thought<sup>39</sup>.

137 Interestingly, in Fig. 1c, the EELS data appears to shift off the substrate-modified calculation and to the free  
 138 space calculation for  $a \leq 3$  nm. Full-wave simulation of Maxwell's equations<sup>46</sup> explains this effect, showing that  
 139 substrate-induced reductions in LSP energy are large for  $a > 3$  nm but vanish for smaller particles. That this feature  
 140 of the data can be qualitatively reproduced in simulations indicates that it is due to retardation and not a quantum  
 141 effect.

142 We now extend the theory to incorporate an optical emitter such as a quantum dot, fluorophore, substrate resonance,  
 143 or second MNP to illustrate how LSP decay to electron-hole pairs is altered in more complex environments. As  
 144 depicted in the inset of Fig. 3, we neglect the emitter's electronic structure and model it as a point dipole oscillating  
 145 at frequency  $\omega_{\text{em}}$  located a distance  $s$  from the MNP surface. Eq. 1 now becomes

$$H_{\text{LSP-em}} = H_{\text{free}} + \left( \frac{V_{\text{em}}}{2} p_{\text{em}}^2 + \frac{\omega_{\text{em}}^2}{2V_{\text{em}}} q_{\text{em}}^2 \right) - \mathbf{d}_{10} \cdot \mathbf{E}_{\text{em}} - \frac{e}{2m_e c} \sum_i [\mathbf{p}_i \cdot \mathbf{A}_{\text{em}}(\mathbf{x}_i) + \mathbf{A}_{\text{em}}(\mathbf{x}_i) \cdot \mathbf{p}_i], \quad (5)$$

146 where  $p_{\text{em}}$  and  $q_{\text{em}}$  are the generalized emitter momentum and coordinate, and  $\mathbf{E}_{\text{em}}$  and  $\mathbf{A}_{\text{em}}$  are the emitter electric  
 147 field and vector potential. The mode volume,  $V_{\text{em}}$ , is defined in connection to the emitter dipole moment, which is  
 148 assumed to be  $\mathbf{d}_{\text{em}} = CV_{\text{em}} p_{\text{em}} \hat{\mathbf{z}}$ , where  $C$  is a dimensionless constant that gives the results below general applicability.  
 149 This Hamiltonian shows that, like the substrate, the emitter couples both to the LSP directly and to individual  
 150 electrons through  $\mathbf{A}_{\text{em}}$ .

151 The direct LSP coupling can again be diagonalized through transformation. This results in two hybridized LSP-  
 152 emitter normal modes with eigenfrequencies defined by

$$\omega_{\pm}^2 = \omega_{\text{em}/10}^2 \cos^2 \theta + \omega_{10/\text{em}}^2 \sin^2 \theta \pm \frac{2g\omega_{10}\omega_{\text{em}}}{\sqrt{V_{10}V_{\text{em}}}} \sin \theta \cos \theta, \quad (6)$$

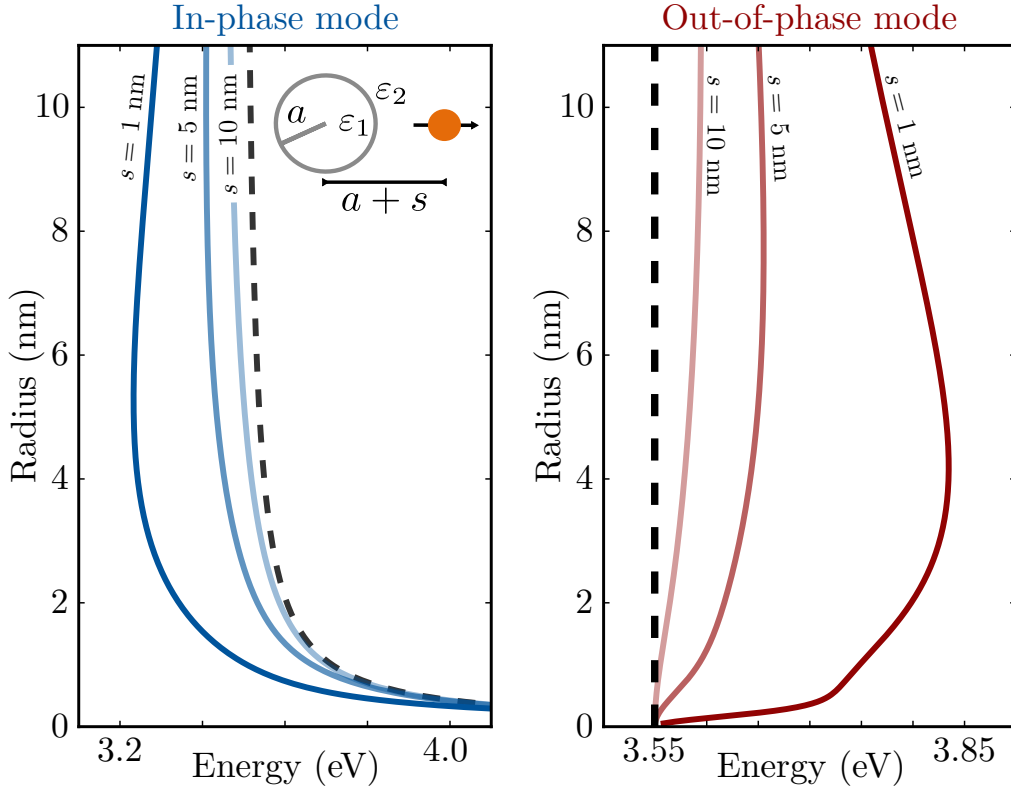


FIG. 3. Evolution of the renormalized in-phase (left) and out-of-phase (right) normal modes of the coupled MNP-optical emitter system (inset) as a function of  $a$  for 3 separation distances,  $s = 1, 5,$  and  $10$  nm. The in-phase mode tracks the uncoupled LSP (left, black dashed line), and shifts to lower energy as the  $s$  decreases. Alternatively, the out-of-phase mode tracks the uncoupled emitter (right, black dashed line) and shifts to higher energy as  $s$  decreases. Further, as the MNP radius decreases, shifting of  $\hbar\omega_{10}$  causes a rapid decoupling of the LSP and emitter, resulting in a rapid redshift of  $\hbar\omega_+^*$ .

153 and mode volumes

$$V_{\pm} = V_{\text{em}/10} \frac{\omega_{\text{em}/10}^2}{\omega_{10/\text{em}}^2} \cos^2 \theta + V_{\text{em}/10} \sin^2 \theta \pm \frac{2g\omega_{\text{em}/10}}{\omega_{10/\text{em}}} \sqrt{\frac{V_{\text{em}/10}}{V_{10/\text{em}}}} \sin \theta \cos \theta. \quad (7)$$

154 Here  $\tan(2\theta) = 2g\omega_{10}\omega_{\text{em}}/\sqrt{V_{10}V_{\text{em}}}(\omega_{\text{em}}^2 - \omega_{10}^2)$ , and  $g = 2CV_{10}V_{\text{em}}(\varepsilon_1 - \varepsilon_2)/\sqrt{12\pi}(a + s)^3$ .

155 The rotation angle  $\theta$  characterizes the degree of mixing between the LSP and emitter and is positive when  $\omega_{\text{em}} > \omega_{10}$ .  
 156 In that case, the  $-$  and  $+$  modes correspond to the well-known in-phase and out-of-phase eigenmodes of a coupled  
 157 dipole system<sup>43,49</sup>. At  $\theta = 0^\circ$ , when  $\omega_{10}$  and  $\omega_{\text{em}}$  are sufficiently detuned or the separation distance  $s$  is much larger  
 158 than  $a$ , the LSP and emitter are essentially uncoupled and the  $-$  mode reduces to the LSP while the  $+$  mode reduces  
 159 to the emitter. On the other hand, if  $\omega_{10}$  and  $\omega_{\text{em}}$  are degenerate or  $s$  is very small,  $\theta$  approaches  $45^\circ$  and the LSP  
 160 and emitter are significantly mixed.

161 This transformation modifies the second coupling term in Eq. 5, and both the in-phase ( $-$ ) and out-of-phase ( $+$ )  
 162 modes interact with electrons differently. Calculating these interaction terms, a perturbation theory can be carried



163 out for each mode, again using  $\mathbf{A}_{\text{em}}(\mathbf{x}_i) \approx \mathbf{A}_{\text{em}}(\langle \mathbf{x}_i \rangle)$ . The resulting decay rates are

$$\begin{aligned}
 \Gamma_-(\omega_-, V_-) &= \left| \frac{\omega_{\text{em}}}{\omega_{10}} \cos \theta - \sqrt{\frac{16\pi V_{\text{em}}}{3V_{10}}} \frac{Ca^3}{(a+s)^3} \sin \theta \right|^2 \Gamma_{\text{free}}(\omega_-, V_-) \\
 \Gamma_+(\omega_+, V_+) &= \left| \sqrt{\frac{V_{10}}{V_{\text{em}}}} \sin \theta + \sqrt{\frac{16\pi}{3}} \frac{\omega_{10}}{\omega_{\text{em}}} \frac{Ca^3}{(a+s)^3} \cos \theta \right|^2 \Gamma_{\text{free}}(\omega_+, V_+).
 \end{aligned}
 \tag{8}$$

164 Notice that the emitter vector potential destructively interferes with the decay in the in-phase configuration where  
 165  $\mathbf{A}$  and  $\mathbf{A}_{\text{em}}$  are misaligned within the particle but constructively interferes in the out-of-phase configuration where  
 166  $\mathbf{A}$  and  $\mathbf{A}_{\text{em}}$  are aligned within the particle. This implies that if the modes are mixed, the out-of-phase mode more  
 167 efficiently decays to electronic excitations than the in-phase mode. This is in stark juxtaposition to the hybridized  
 168 modes' coupling to near-field energy transfer and far-field radiation, where the in-phase mode's larger dipole moment  
 169 makes it the more efficiently decaying hybrid resonance<sup>43</sup>.

170 Eq. 8 can be used just as the decay rates previously to calculate the quantum-corrected eigenenergies,  $\hbar\omega_{\pm}^*$ . For the  
 171 case where the emitter is another silver nanosphere with fixed radius (4 nm,  $\hbar\omega_{\text{em}} = 3.55$  eV), we plot in Fig. 3 the  
 172 eigenenergies as a function of  $a$  for three separation distances,  $s = 1, 5,$  and 10 nm, and we compare to the uncoupled  
 173 ( $g = 0$ ) energies (black dashed curves). We see that  $\hbar\omega_-^*$  qualitatively tracks the LSP and shifts to lower energy as  $s$   
 174 decreases, with a maximal shift when  $\omega_{10} \sim \omega_{\text{em}}$ . On the other hand,  $\hbar\omega_+^*$  tracks  $\hbar\omega_{\text{em}}$  and shifts to higher energy as  
 175  $s$  decreases.

176 Interestingly, as  $a$  decreases, the shift of the in-phase mode becomes severe enough that the LSP and emitter  
 177 effectively decouple, and the out-of-phase mode rapidly collapses back to the uncoupled emitter energy, giving it  
 178 a dramatically different  $a$ -dependence. This pronounced change highlights previously unexplored quantum effects  
 179 on plasmon hybridization. Measurement of the hybridized LSP-emitter modes' dependence on MNP size would  
 180 support the prediction that the out-of-phase mode more effectively couples to electrons, suggesting new strategies to  
 181 disentangle LSP decay pathways.

## 182 I. CONCLUSION

183 In this paper we have developed an analytic theory of noble metal LSPs in optically-active environments. By incor-  
 184 porating dielectric environment effects on LSP-electron interaction, our theory agrees with Mie theory<sup>48</sup>, photofrag-  
 185 mentation spectroscopy<sup>36</sup>, matrix deposition spectroscopies<sup>37,38</sup>, and EELS<sup>39</sup> over orders-of-magnitude changes in size  
 186 with only two parameters defined by bulk dielectric data<sup>45</sup>, indicating that environmental effects play a significant  
 187 role in plasmonic Landau damping.

188 Current work on optimizing plasmonic systems for charge manipulation often relies on indirect, spectral signals  
 189 to elucidate nanoscale behavior. Experiments are in turn required to design systems which isolate Landau damping  
 190 from other decay pathways such as near-field energy transfer and far-field radiation. Our approach disentangles LSP-  
 191 electron and LSP-photon interactions by showing that the out-of-phase mode of a hybrid LSP-emitter system more  
 192 strongly couples to electrons while the in-phase mode more strongly couples to photons. As a whole, this work shows  
 193 that just as LSP radiative properties are strongly environmentally dependent, LSP decay to electron-hole pairs can  
 194 be suppressed or enhanced by environmental factors. Our approach therefore provides an analytic platform to tailor

195 the optoelectronic properties of open plasmonic systems.

196

## ACKNOWLEDGMENTS

197 We thank D. Rim for useful discussions regarding the mathematics, S. C. Quillin for assistance with the numerical  
 198 simulations, and Prof. H. Petek for critically reading and editing the manuscript. This work was partially supported  
 199 by the NSF under award numbers DGE-1256082 (N.T.) and CHE-1253775 (D.J.M.).

200 \* thakkar@uw.edu

201 † masiello@chem.washington.edu

202 <sup>1</sup> W. L. Barnes, A. Dereux, and T. W. Ebbesen, *Nature* **424**, 824 (2003).

203 <sup>2</sup> R. F. Oulton, V. J. Sorger, D. Genov, D. Pile, and X. Zhang, *Nature Photonics* **2**, 496 (2008).

204 <sup>3</sup> G. Baffou and R. Quidant, *Laser & Photonics Reviews* **7**, 171 (2013).

205 <sup>4</sup> G. Baffou, R. Quidant, and F. J. García de Abajo, *ACS Nano* **4**, 709 (2010).

206 <sup>5</sup> M. L. Brongersma, N. J. Halas, and P. Nordlander, *Nature Nanotechnology* **10**, 25 (2015).

207 <sup>6</sup> S. F. Tan, L. Wu, J. K. Yang, P. Bai, M. Bosman, and C. A. Nijhuis, *Science* **343**, 1496 (2014).

208 <sup>7</sup> S. Linic, P. Christopher, and D. B. Ingram, *Nature Materials* **10**, 911 (2011).

209 <sup>8</sup> W. Du, T. Wang, H.-S. Chu, L. Wu, R. Liu, S. Sun, W. K. Phua, L. Wang, N. Tomczak, and C. A. Nijhuis, *Nature*  
 210 *Photonics* **10**, 274 (2016).

211 <sup>9</sup> L. D. Landau, *Zh. Eksp. Teor. Fiz.* **10**, 25 (1946).

212 <sup>10</sup> K. Wu, J. Chen, J. McBride, and T. Lian, *Science* **349**, 632 (2015).

213 <sup>11</sup> V. Schweikhard, A. Grubisic, T. A. Baker, I. Thomann, and D. J. Nesbitt, *ACS Nano* **5**, 3724 (2011).

214 <sup>12</sup> A. Hoggard, L.-Y. Wang, L. Ma, Y. Fang, G. You, J. Olson, Z. Liu, W.-S. Chang, P. M. Ajayan, and S. Link, *ACS Nano*  
 215 **7**, 11209 (2013).

216 <sup>13</sup> G. Li, C. Cherqui, N. W. Bigelow, G. Duscher, P. J. Straney, J. E. Millstone, D. J. Masiello, and J. P. Camden, *Nano*  
 217 *Letters* **15**, 3465 (2015).

218 <sup>14</sup> E. M. Purcell, *Physical Review* **69**, 681 (1946).

219 <sup>15</sup> R. Chance, A. Prock, and R. Silbey, *Adv. Chem. Phys.* **37**, 65 (1978).

220 <sup>16</sup> A. Kawabata and R. Kubo, *Journal of the Physical Society of Japan* **21**, 1765 (1966).

221 <sup>17</sup> W. A. Kraus and G. C. Schatz, *The Journal of Chemical Physics* **79**, 6130 (1983).

222 <sup>18</sup> U. Kreibig and L. Genzel, *Surface Science* **156**, 678 (1985).

223 <sup>19</sup> C. Yannouleas and R. A. Broglia, *Annals of Physics* **217**, 105 (1992).

224 <sup>20</sup> G. Weick, R. A. Molina, D. Weinmann, and R. A. Jalabert, *Physical Review B* **72**, 115410 (2005).

225 <sup>21</sup> R. C. Monreal, T. J. Antosiewicz, and S. P. Apell, *New Journal of Physics* **15**, 083044 (2013).

226 <sup>22</sup> G. Toscano, J. Straubel, A. Kwiatkowski, C. Rockstuhl, F. Evers, H. Xu, N. A. Mortensen, and M. Wubs, *Nature Commu-*  
 227 *nications* **6** (2015).

228 <sup>23</sup> A. Brandstetter-Kunc, G. Weick, D. Weinmann, and R. A. Jalabert, *Physical Review B* **91**, 035431 (2015).

229 <sup>24</sup> P. Echenique, J. Pitarke, E. Chulkov, and A. Rubio, *Chemical Physics* **251**, 1 (2000).

230 <sup>25</sup> A. García-Lekue, J. M. Pitarke, E. V. Chulkov, A. Liebsch, and P. M. Echenique, *Physical Review B* **68**, 045103 (2003).

231 <sup>26</sup> R. Sundararaman, P. Narang, A. S. Jermyn, W. A. Goddard III, and H. A. Atwater, *Nature Communications* **5** (2014).

- 232 <sup>27</sup> M. Bernardi, J. Mustafa, J. B. Neaton, and S. G. Louie, *Nature Communications* **6** (2015).
- 233 <sup>28</sup> H. Haberland, *Nature* **494**, E1 (2013).
- 234 <sup>29</sup> X. Chen, J. E. Moore, M. Zekarias, and L. Jensen, *Nature Communications* **6** (2015).
- 235 <sup>30</sup> J. Lermé, *The Journal of Physical Chemistry C* **115**, 14098 (2011).
- 236 <sup>31</sup> K.-Y. Lian, P. Salek, M. Jin, and D. Ding, *The Journal of Chemical Physics* **130**, 174701 (2009).
- 237 <sup>32</sup> C. M. Aikens, S. Li, and G. C. Schatz, *The Journal of Physical Chemistry C* **112**, 11272 (2008).
- 238 <sup>33</sup> V. Bonačić-Koutecky, V. Veyret, and R. Mitrić, *The Journal of Chemical Physics* **115**, 10450 (2001).
- 239 <sup>34</sup> K. Yabana and G. F. Bertsch, *Physical Review A* **60**, 3809 (1999).
- 240 <sup>35</sup> U. Kreibig and M. Vollmer, *Optical properties of metal clusters*, Vol. 25 (Springer Science & Business Media, 2013).
- 241 <sup>36</sup> J. Tiggesbäumker, L. Köller, K.-H. Meiwes-Broer, and A. Liebsch, *Physical Review A* **48**, R1749 (1993).
- 242 <sup>37</sup> K.-P. Charlé, L. König, S. Nepijko, I. Rabin, and W. Schulze, *Crystal Research and Technology* **33**, 1085 (1998).
- 243 <sup>38</sup> W. Harbich, S. Fedrigo, and J. Buttet, *Zeitschrift für Physik D Atoms, Molecules, and Clusters* **26**, 138 (1993).
- 244 <sup>39</sup> J. A. Scholl, A. L. Koh, and J. A. Dionne, *Nature* **483**, 421 (2012).
- 245 <sup>40</sup> L. Zhou, Y. Tan, J. Wang, W. Xu, Y. Yuan, W. Cai, S. Zhu, and J. Zhu, *Nature Photonics* (2016).
- 246 <sup>41</sup> A. G. Curto, G. Volpe, T. H. Taminiau, M. P. Kreuzer, R. Quidant, and N. F. van Hulst, *Science* **329**, 930 (2010).
- 247 <sup>42</sup> C. L. Haynes, A. D. McFarland, and R. P. Van Duyne, *Analytical Chemistry* **77**, 338 (2005).
- 248 <sup>43</sup> N. Thakkar, C. Cherqui, and D. J. Masiello, *ACS Photonics* **2**, 157 (2015).
- 249 <sup>44</sup> S. Lecoultre, A. Rydlo, and C. Félix, *The Journal of Chemical Physics* **126**, 204507 (2007).
- 250 <sup>45</sup> P. B. Johnson and R. W. Christy, *Physical Review B* **6**, 4370 (1972).
- 251 <sup>46</sup> See supplemental material at [URL] for a complete derivation of all the presented results.
- 252 <sup>47</sup> C. Cherqui, N. Thakkar, G. Li, J. P. Camden, and D. J. Masiello, *Annual Review of Physical Chemistry* **67**, 331 (2016).
- 253 <sup>48</sup> G. Mie, *Annalen der Physik* **330**, 377 (1908).
- 254 <sup>49</sup> E. Prodan, C. Radloff, N. J. Halas, and P. Nordlander, *Science* **302**, 419 (2003).